Plastic 3D-printing in adsorption cooling: a proof-of-principle module

Plastic 3D-printing in adsorption cooling: a proof-of-principle module

Shihab AL-Hasni, Giulio Santori*

The University of Edinburgh, School of Engineering, Institute for Materials and Processes, Sanderson Building, The King's Buildings, Mayfield Road, EH9 3BF, Edinburgh, Scotland, UK

*Corresponding author: g.santori@ed.ac.uk

Abstract

Plastic 3D–printing allows the replacement of metal parts in a water/silica-gel adsorption heat transformer module and its rapid manufacturing at low-cost. This research investigates a simple design using three finned metal heat exchangers enclosed in one plastic 3D printed vessel. The dynamics of a conventional packed bed adsorber of Siogel silica gel grains with thermal response method is first identified, to establish a benchmark case and allow to focus only on the challenges introduced by plastic 3D–printing. Final testing of the device across a range of operating conditions and cycle times representative of cooling, desalination and intermediate shows the adsorber follows an unconventional thermodynamic cycle. Generation of larger powers is achievable by coupling multiple small modules.

Introduction

In an energy system that is changing, moving from the adoption of traditional to emerging technologies, heat is still a major player, regardless of whether it is a need or as a waste. District heating and cooling, network stability and data centres are only a few examples of the applications in which heat is delivered, managed, converted and emitted across different temperatures. Adsorption heat transformer has the unrivalled capability of transforming (shifting or amplifying) heat across the temperature scales. Adsorption heat transformation processes are especially suited for converting heat at a temperature only few degrees above ambient (ultralow grade heat) into cooling (adsorption chillers), showing in some instances encouraging second-law efficiencies >0.9,[1–3] while consuming modest amounts of electricity. The distinctive feature of usefully converting heat usually meant useless, makes adsorption chillers a key technology for the decarbonisation of those sectors where the emission of low-

grade heat or the generation of low temperature renewable heat is co-located with the need for cooling. By using in most cases water as refrigerant, the adoption of this technology has no effect on the ozone layer, a part from the environmental impact from the whole life cycle. The operation of a standard adsorption heat chiller needs two heat sources and one heat sink, at different temperatures. The heat sources at highest temperature T_{hot} (e.g. 50-80°C) and lowest temperature T_{ev} (e.g. 12-18°C) power the heat transformer, which discharges heat at temperature T_{cond} close to ambient. The thermodynamic cycles and operation of the adsorption heat transformation process for cooling are more extensively detailed elsewhere.[4–6] Commercial adsorption chillers are available from manufacturers such as Fahrenheit GmbH, Mayekawa Mfg. Co. Ltd, BryAir Pvt Ltd and Sorption Technologies GmbH which sell them in modular units with cooling power ranging from 8kW (recently discontinued) to 1180kW in a niche market.[7–9] Research in adsorption cooling has primarily focused on performance enhancement, with little attention to the assessment of whether advanced solutions would be economically viable and beneficial for competition in the price-sensitive market of heat-powered chillers, already dominated by absorption chillers. Although they share numerous characteristics, adsorption and absorption cooling technologies convert heat from sources in distinct temperature ranges, with adsorption being the only cooling process able to generate a cooling effect when $T_{hot} < 70$°C.[3,10,11] Fig. 1 reports a comparison on the specific price (€ per kW of cooling) and on volumetric power density (kW of cooling per m^3 installed). Although small, the gap between the technologies is visible, with adsorption chillers having currently lower energy density and higher price than absorption chillers.

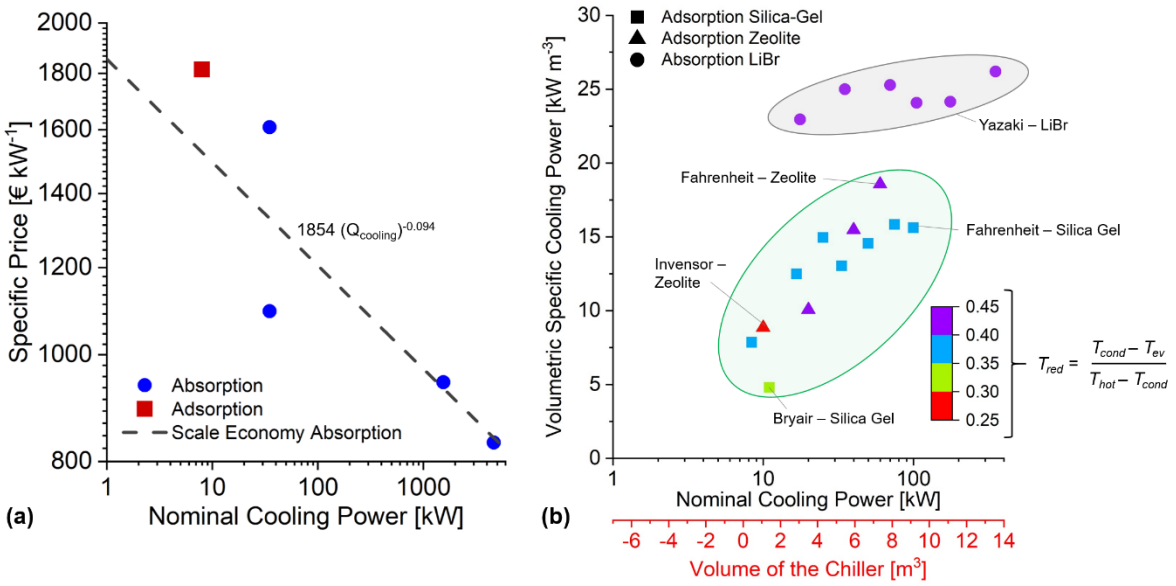

Figure 1: Comparison between adsorption and absorption chillers (a) on the specific price (€ per kW of cooling) and (b) volumetric power density (kW of cooling per m^3 installed) from open disclosed data. In (a), the scale economy correlation for absorption chillers is from regression of data,[12–14] compared with the only disclosed and verified data for adsorption chiller.[15] Data disclosed in different years have been reconciled to 2020 by using the Chemical Engineering Plant Cost Index –Equipment. In (b), all data are from technical datasheets of the respective companies.

Fig. 1 indicates that absorption chillers remain the more cost-effective investment option among the heat-powered cooling technologies.

3D printing is promising of immense benefits to adsorption chiller due to low cost of manufacturing and equipment (predicted to drop from 50% to 75% over the next decade)[16], freedom of choice of the adsorption module shape and easiness of fabrication directly from a computer-aided-design model. Plastic 3D printing has been trialled in adsorption heat transformation in custom heat exchangers maximising heat and mass transfer.[17] Although 3D printed structures have been characterised, operation in adsorption chillers has never been trialled for the inescapable challenge of maintaining the vacuum while working with 3D printed structures.

This study pioneers the utilisation of 3D printing in a small module of adsorption chiller and builds upon a previous pilot investigation in which the same research group has demonstrated how stereo lithography (SLA) 3D printing can manufacture vacuum and pressure-tight polymer vessels.[18] The module demonstrated in this study uses the most common silica gel grains-water working pair to facilitate the comparison of the performance with other designs[19] and do

not distract from the main objective of this research: proving whether 3D printing can be a viable manufacturing technology for the sector. The scale of the device demonstrated in this investigation is small to meet: (i) the intention of pushing the boundary of modularity in the design, achieving higher power by repeating several time the same unit and benefitting from the advantages of modularity brings along; (ii) the build space available in the 3D printer.

The module assembly and its cost of manufacturing

The module consists of three aluminium heat exchangers in a 3D-printed enclosure. The choice of 3D-printing only the enclosure arises from the numerous challenges posed by plastics in an application operating with liquid water and water vapour under vacuum and from the special design of heat transformer proposed. Limiting the 3D-printing to the only enclosure allowed to focus on all the plastic-related issues only, free from those related to the heat and mass transfer optimisation, which would otherwise be overshadowed by the 3D printing challenges. The 3D printed vacuum-tight plastic vessel (Fig. 2) encloses three vertically mounted aluminium heat exchangers (RC Racing Radiators, Italy) with similar features. The upper heat exchanger is packed with silica gel (adsorber) and flipped, the middle heat exchanger is for heat rejection to the ambient (condenser), and the bottom heat exchanger is a flooded evaporator. The module has external dimensions of 11.7 cm x 9.5 cm x 5.4 cm and internal volume of 355 cm^3. Such a small volume is for facilitating the experiments and for the limited building volume available in the 3D-printer. The steps followed for fabricating the module and the test rig for its characterisation are available in the Supplemental Information. The water loops used in this study are the same already used in [19].

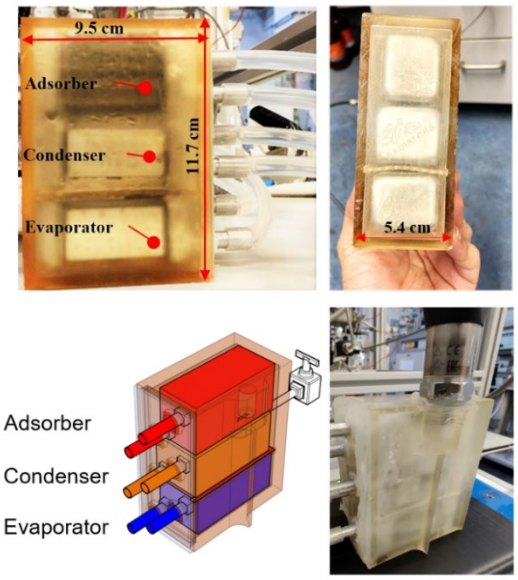

Figure 2: the 3D printed adsorption chiller module.

Plastic 3D printing can reduce the cost of manufacturing adsorption chiller significantly. The same method and tools used elesewhere[9] were applied to cost the vessel produced in this study and compare it with an equivalent stainless steel vessel (Table 1). Using a 3D printed vessel instead of stainless steel can bring up savings for up to 3.9 times when further to the direct material all concerned manufacturing costs are taken into account.

Table 1: Manufacturing cost comparison between welding of stainless steel and 3D-printed plastic of the vessel in this study

	Direct Material [€]	Direct Labour [€]	Manufacturing Overhead [€]	Total Cost [€]	Total Weight [kg]
Stainless steel	24.11	147.56	93.52	267.19	5.2
3D printed plastic	12.54	14.24	42.06	68.83	0.1

Note: manufacturing of metal vacuum-tight vessels requires skilled workforce for welding and special vacuum fittings. 3D printing shows different types of manufacturing costs from the database of CALC4XL[20].

Static properties of the adsorber, condenser and evaporator heat exchangers

The module contains three finned Aluminium heat exchangers (HEXs) of the type in Fig. 3 having almost identical static characteristics. One of the three heat exchangers was used as an adsorber after packing it with grains of Siogel silica-gel of 1mm average diameter.

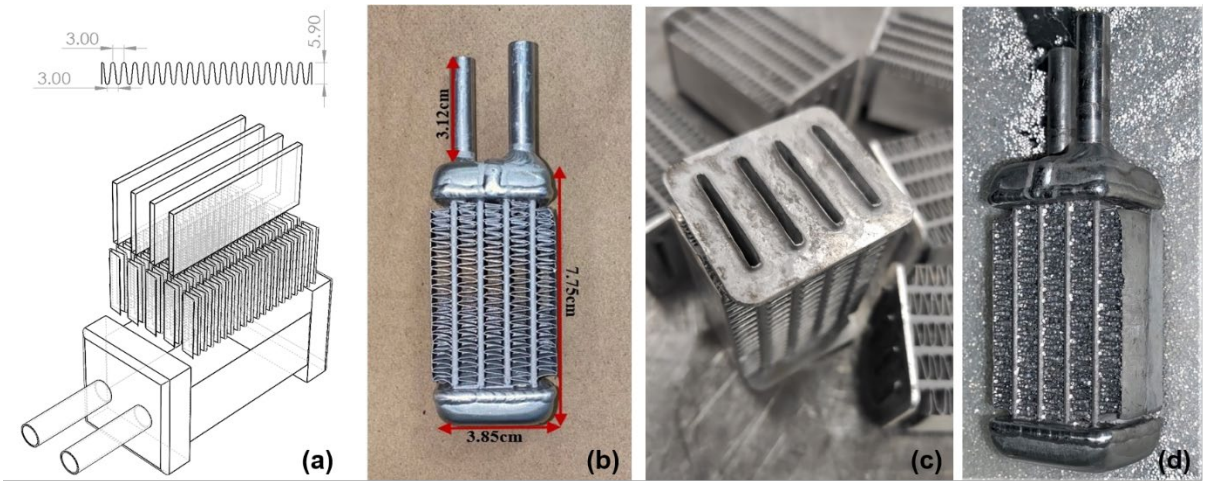

Figure 3: geometrical features of the Aluminium heat exchangers of this study. All heat exchangers have fins height 5.9 mm and pitch 3.0 mm. The heat transfer surface area of each heat exchanger is 0.093 m^2. The adsorber, packed with Silica gel grains, is in (d).

The static thermal characteristics of the heat exchangers are instrumental in the identification of the sensible heat absorbed by them, essential for the analysis of how the energy partition in the adsorber between sensible heat and heat of adsorption, when it undergoes large temperature changes. The static characteristics are less important in the condenser and evaporator, where the changes of inlet and outlet temperatures are small. There is little consistency in previous investigations on the static thermal characteristics of the heat exchangers and measurement methodologies are not standardised yet. As a result, diverse designs are difficult to compare. Gluesenkamp et. al [21] proposed the concept of thermal mass [J K^{-1}], applying it to the adsorber. The thermal mass is defined as sum of all the individual items composing the heat transfer unit (the heat capacity of the heat transfer fluid, of the metal parts and of the adsorption material). However, there is always a discrepancy between this value and the actual thermal mass, since the adsorber always shows temperature gradients even at steady state and this can be large especially across the adsorption material if it comes in multiple layers of grains. The identification of the actual thermal mass requires dedicated experiments starting with measuring the thermal response of the heat exchanger to a temperature step from an initial temperature until a steady-state temperature. The identification of dynamic systems through measurement of the response from a step-input is a very well established method applied in diverse engineering fields. For a heat exchanger perfectly insulated from the surroundings, the following holds:

$$\tau_{HEX} \frac{dT_{HEX}(t)}{dt} = [T_{in} - T_{out}(t)]_{exp} \quad (1)$$

$$\tau_{HEX} = \frac{(m\, c_p)_{HEX}}{(\dot{m}\, c_p)_{htf}} \quad (2)$$

where the variable T_{HEX} [K] is a time-dependent overall temperature of the heat exchanger, $(T_{in} - T_{out})_{exp}$ [K] is the time-dependent difference between inlet and outlet temperature of the heat transfer fluid measured experimentally, τ_{HEX} [s] is the ratio between the actual heat capacity of the heat exchanger $(mc_p)_{HEX}$ and the heat capacity rate $(\dot{m}c_p)_{htf}$ of the heat transfer fluid. τ_{HEX} is an experimental parameter determined through regression of the results from temperature-step experiments. Fig. 4 reports the results of these tests, performed under vacuum, after installation of the adsorber heat exchanger in the 3D-printed vessel, to make the heat losses negligible. From an initial temperature of 23.4°C, the inlet temperature of the heat transfer fluid (T_{in}) step-changes according to the following three ranges: (23.4°C → 38.0°C; 23.4°C → 47.3°C; 23.4°C → 56.7°C) while the time-variant outlet temperature of the heat transfer fluid $T_{out}(t)$ is acquired. Therefore, the value of the quantity $[T_{in} - T_{out}(t)]_{exp}$ is known in each instant. By integrating eq. (1) from the time t_0, at the beginning of the temperature step, to the time t_{end}, when the stead-state is achieved (4100 s in this case), gives:

$$\tau_{HEX} \int_{T_{HEX}(t_0)}^{T_{HEX}(t_{end})} dT_{HEX}(t) = \int_{t_0}^{t_{end}} [T_{in} - T_{out}(t)]_{exp}\, dt \quad (3)$$

We call N_1, N_2 and N_3 the quantities resulting from the integral $\int_{t_0}^{t_{end}} [T_{in} - T_{out}(t)]_{exp}\, dt$ in each experimental temperature step from the temperature step 1 (23.4°C → 38.0°C) to the temperature step 3 (23.4°C → 56.7°C). If the temperature step is small:

$$\int_{T_{HEX}(t_0)}^{T_{HEX}(t_{end})} dT_{HEX}(t) \sim [T_{in}(t_0) - T_{in}(t_{end})] = \Delta T_{in} \quad (4)$$

By writing eq. (3) for the three temperature steps ($\Delta T_{in,1}$ = 14.6°C; $\Delta T_{in,2}$ = 23.9°C; $\Delta T_{in,3}$ = 33.4°C), τ_{HEX} is obtained as:

$$\tau_{HEX} = \frac{N_1}{\Delta T_{in,1}} = \frac{N_2}{\Delta T_{in,2}} = \frac{N_3}{\Delta T_{in,3}} \quad (5)$$

τ_{HEX} is the slope of a straight line having intercept in the origin and passing through the coordinates ($\Delta T_{in,1}$, N_1), ($\Delta T_{in,2}$, N_2) and ($\Delta T_{in,3}$, N_3). The linear regression in Fig. 4 shows a

τ_{HEX} of 4.78 s. τ_{HEX} is a time constant of the heat exchanger and represents the time needed for 1kg of heat exchanger to increase its temperature of 1°C at the specific experimental flow rate.

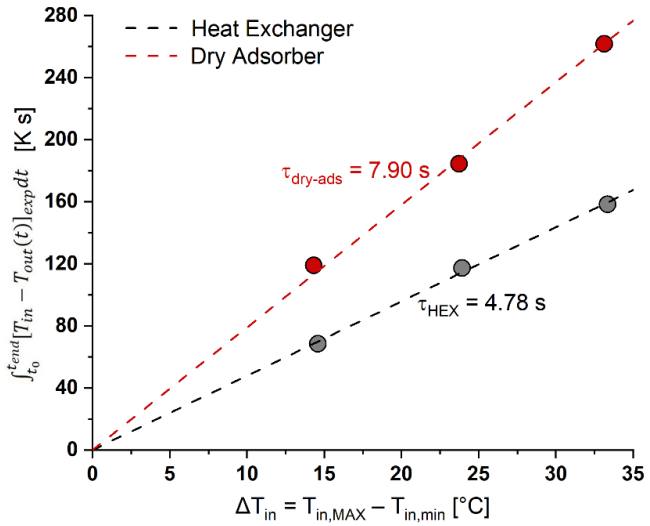

Figure 4: regression leading to the identification of τ_{HEX} = 4.78 s and $\tau_{dry-ads}$ = 7.90 s

The heat capacity rate of the heat transfer fluid $(\dot{m}c_p)_{htf}$ remains constant at 27.9 W K^{-1} since its major contributor, the heat capacity of the heat transfer fluid (water), does not change significantly in the experimental temperature ranges. From eq. (2) and τ_{HEX}, the heat capacity of the overall heat exchanger including the water inside (or thermal mass) is 133.4 J K^{-1}, slightly lower than 147.6 J K^{-1} resulting from the sum of the individual contribution of water and aluminium alloy as previously proposed for the identification of the heat exchanger thermal mass.[21] The discrepancy is likely due to the uncertainty on the actual aluminium alloy and on the presence of an amount of welding material, which is not negligible given the small size of the heat exchangers in Fig. 3. Table 2 collects all the static characteristics of the three heat exchangers used in this study.

Table 2: static characteristics and NTUs of the heat exchangers used in the adsorption chiller (Fig. 3).

	Adsorber Heat exchanger	Condenser	Evaporator	
Metal (Aluminium) weight [g]	47.10 ± 0.05	45.39 ± 0.05	40.67 ± 0.04	Measured
Water weight [g]	26.10 ± 0.03	25.13 ± 0.03	22.51 ± 0.02	Measured
Total weight [g]	73.20 ± 0.10	70.52 ± 0.10	63.18 ± 0.08	Measured
Metal Heat Capacity [J K^{-1}]	42.40 ±1.17	40.90 ±1.13	36.60 ±1.03	Calculated
Water Heat Capacity [J K^{-1}]	109.2 ± 0.11	105.1 ± 0.11	94.10 ± 0.09	Calculated
Heat exchanger time constant [s]	4.78 ± 0.27			
Actual thermal mass [J K^{-1}]	133.4 ± 7.7	--	--	Measured
Water flowrate [litre min^{-1}]	0.40 ± 0.01	0.80 ± 0.02	0.40 ± 0.01	Measured
Water average velocity [m s^{-1}]	0.1	0.1-0.2	0.1	Calculated*
Heat transfer surface area (external) [m^2]	0.093	0.093	0.093	Calculated

*Results from computational fluid dynamic simulation of the heat exchanger

Dynamics of the dry adsorber

The packed bed adsorber contains 20 g of Siogel silica gel in beads, secured with a 290 µm polymer mesh (Plastok Meshes & Filtration Ltd, UK) having 50% open area. The addition of silica gel changes the static and dynamic characteristics of the adsorber, requiring additional thermal response experiments in which, similarly to the previous experiments, the dry adsorber undergoes temperature steps. Eq. (1) can be applied again to the whole dry adsorber:

$$\tau_{dry-ads}\frac{dT_{dry-ads}(t)}{dt} = [T_{in} - T_{out}(t)]_{exp} \quad (6)$$

$$\tau_{dry-ads} = \frac{(m\, c_p)_{dry-ads}}{(\dot{m}\, c_p)_{htf}} \quad (7)$$

where the variable $T_{dry\text{-}ads}$ [K] is the time-dependent overall temperature of the adsorber without adsorption (dry condition) and $(T_{in} - T_{out})_{exp}$ [K] are as in the previous experiment the measured values of inlet and outlet temperature of the heat transfer fluid (water), $\tau_{dry\text{-}ads}$ is the ratio between the actual heat capacity of the dry adsorber $(mc_p)_{dry\text{-}ads}$ and the heat capacity rate $(\dot{m}c_p)_{htf}$ of the heat transfer fluid (water). $\tau_{dry\text{-}ads}$ is determined through regression of the results from temperature step experiments encompassing both transient and steady-state. The measurements were taken under vacuum and with the adsorber installed directly in the 3D-printed vessel in absence of internal water refrigerant to avoid adsorption. Given the presence of high-vacuum, the temperature of the adsorption material must get identical to the temperature of the heat exchanger if a sufficiently long time for equalising the local

temperatures across the dry adsorber is allowed. Fig. 4 shows the dry adsorber time-constant of $\tau_{dry\text{-}ads}$ = 7.90 s, resulting from the three temperature step experiments. The heat capacity rate of the heat transfer fluid $(\dot{m}c_p)_{htf}$ is still 27.9 W K^{-1} as previously, given the closeness of the temperature steps. The combination of these two values provides a heat capacity of the dry adsorber of 220.3 J K^{-1}. Table 3 collects a comparison between the values obtained from this experiment and with benchmarking values from similar type of adsorbers.[21] The benchmark has dimensions one order of magnitude larger than the one in this study but specific values remains the same across the scales.

Table 3: static characteristics of the dry adsorber (Fig. 3, first from the right) and comparison with benchmarking data.

	Dry Adsorber	Flat tube–fin, packed benchmark*
Silica gel weight (m_{sg}) [g]	20.0 ± 0.02	310
Total dry adsorber weight ($m_{dry\text{-}ads}$) [g]	93.0 ± 0.10	1120
Calculated Silica gel heat capacity [J K^{-1}]	0.007	
Calculated dry adsorber heat capacity [J K^{-1}]	0.149	1.92
Metal: Total weight ratio	0.50	
Water: Total weight ratio	0.28	
Silica gel: Total weight ratio	0.22	0.28
Dry adsorber time constant ($\tau_{dry\text{-}ads}$)	7.90 ± 0.44	--
Dry adsorber heat capacity [J K^{-1}]	220.3 ± 12.83	--
Dry adsorber heat capacity per mass of adsorption material [kJ K^{-1} kg$_{silica\ gel}^{-1}$]	11.02 ± 0.30	6.10
Dry adsorber specific heat capacity [kJ K^{-1} kg$_{dry\text{-}ads}^{-1}$]	2.37	1.70
Heat exchanger (water+metal): Dry adsorber heat capacity ratio	0.61	

Note: *benchmarking data for a flat tube-fin packed silica gel adsorber using water as heat transfer fluid.[21]

The dry adsorber in this study has specific heat capacity 1.4 times higher than the benchmark (2.37 kJ K^{-1} kg$_{dry\text{-}ads}^{-1}$ vs. 1.70 kJ K^{-1} kg$_{dry\text{-}ads}^{-1}$), whose 60% comes from the heat exchanger specific heat capacity. Table 1 shows that the main contributors to the heat exchanger heat capacity is the amount of heat transfer fluid (water), located mostly in the manifolds at the two ends of the heat exchanger core. The two manifolds contain about 80% of the water in the heat exchanger. Minimisation of the manifold volumes can reduce the heat capacity of the adsorber to values aligned with the benchmark, reduce the time constant and the sensible heat losses, increasing the performance of the whole unit.

Energy Balance of the wet adsorber

Although useful for obtaining static thermal characteristics, eqns (1) to (7) cannot be directly applied to the analysis of the module dynamics — with adsorption and desorption occurring. The heat of adsorption and the presence of a variable amount of water in the adsorption material make the energy balance equation non–linear. Given the principle of superimposition applies only to linear differential equations, the simple subtraction of the energy consumed by the dry adsorber from the total energy during (wet) operation, as occasionally done in some applications of the thermal response experiment,[22,23] would lead to incorrect conclusions. The dynamic response of an adsorber in operation (wet adsorber) requires re-writing of the energy balance in a way that the contribution of the dry adsorber from eq. (6) is clearly identifiable and isolatable from the rest of the contributions. Under the main assumptions of: *(i)* negligible water vapour–adsorption material convective heat transfer; *(ii)* negligible internal energy accumulation in the ideal gas phase; *(iii)* equivalence between the specific heats of saturated liquid water and adsorbed water vapour; *(iv)* negligible contribution of the term $q(t)\, dh_{ads}(t)$; *(v)* The adsorber is homogeneous in temperature (no thermal gradients are present in the adsorber), the following balance applies (Supplemental Information show how to derive eq. (8)):

$$\left[\tau_{dry-ads} + \left(\frac{\tau_{dry-ads}}{c_{p,eff,dry-ads}} - \frac{\tau_{HEX}}{c_{p,effHEX}}\right) c_{p,satliq,w} q(t)\right] \frac{dT(t)}{dt} - \tau_{dry-ads} \frac{h_{ads}(t)}{c_{p,sg,dry}} \frac{dq(t)}{dt} = [T_{in}(t) - T_{out}(t)]_{exp} \quad (8)$$

Where $T(t)$ is the time-dependent overall adsorber temperature [K], $q(t)$ is the time-dependent uptake [$mol_{water}\ kg_{silica\ gel}^{-1}$], $c_{p,satliq,w}$ and $c_{p,eff,dry-ads}$ and $c_{p,eff,HEX}$ are the specific heat capacities of saturated liquid water [$J\ mol_{water}^{-1}\ K^{-1}$], of the dry adsorber [$J\ kg^{-1}\ K^{-1}$] (in Table 2) and of the heat exchanger [$J\ kg^{-1}\ K^{-1}$] (in Table 1), and h_{ads} is the differential heat of water adsorption on Siogel silica gel [$J\ mol_{water}^{-1}$].

Eq. (8) can be used to assess how heat is distributed in the adsorber from thermal response experimental data (i.e. the experimental time-variant temperature difference $[T_{in} - T_{out}]_{exp}$). In Eq. (8), the contributions of sensible and non-sensible heat are clearly separable.

Unfortunately, the amount adsorbed in not a quantity measured directly and has to be assessed with appropriate equilibrium and kinetic models as discussed below.

Eq. (8) is a non–linear differential algebraic equation because of the terms $\left(\frac{\tau_{dry-ads}}{c_{p,eff,dry-ads}} - \frac{\tau_{HEX}}{c_{p,effHEX}}\right) c_{p,satliq,w} q(t) \frac{dT(t)}{dt}$ and $\tau_{dry-ads} \frac{h_{ads}(t)}{c_{p,sg,dry}} \frac{dq(t)}{dt}$. The feature renders the principle of superimposition inapplicable — the contribution to the overall energy consumed cannot be assessed by subtracting the energy eq. (6) from the total measured, since eq. (6) is a linear differential equation while the measured powered exchanged follows the non–linear dynamics represented by eq. (8).

Equilibrium and Kinetics of Siogel silica gel

The following two equations must be added to suit the unmeasured unknown *q(t)* in eq. (8):

$$ln\left(\frac{q_{eq}(t)}{q_s}\right) = -\left[\frac{RT(t)}{E} ln\left(\frac{P_{sat}(T(t))}{P_{exp}(t)}\right)\right]^n \quad (9)$$

$$\frac{dq(t)}{dt} = K\left(q_{eq}(t) - q(t)\right) \quad (10)$$

where *q(t)* is the actual time-dependent uptake [mol_{water} $kg_{sg,dry}^{-1}$], $q_{eq}(t)$ [mol_{water} $kg_{sg,dry}^{-1}$] is the time dependent equilibrium uptake from eq. (9), the Dubinin–Astakhov isotherm, with parameters {q_s; E; n} = {21.1 mol_{water} $kg_{sg,dry}^{-1}$; 3.96 kJ mol_{water}^{-1}; 1.1}[24] [25], P_{sat} [kPa] is the saturation pressure of water at the adsorber temperature T, P_{exp} [kPa] the experimental pressure acquired during the tests. Eq. (10) is an empirical linear model relying on experimental data collected on the specific material. No open data exist on direct measurement of the mass transfer coefficient K [s^{-1}] of the Siogel silica gel used in this study. However, Brandani and Mangano [26] reviewed the mass transfer coefficient K for a number of different silica gels, highlighting how the data of mass transfer coefficient from different laboratories all vary in a narrow range. Data measured by Brandani and Mangano [26], with zero length column technique, and Goyal et al. [27] refer to silica gels having average pore of size 2 nm as in the case of Siogel silica-gel in this study. Goyal et al. [27] provide the following temperature dependence of the mass transfer coefficient K:

$$K = \frac{15}{R_p^2} D_{s,0} e^{-E_a/RT(t)} \quad (11)$$

Where $D_{s,0}$ = 9.15 10^{-10} m^2 s^{-1} is the pre-exponential constant, E_a = 2.22 kJ mol^{-1} is the activation energy and R = 0.0083145 is the universal gas constant [kJ mol^{-1} K^{-1}]. Brandani and Mangano [26] show instead that the mass transfer coefficient changes with temperature and concentration in beads having effective diameter 1.84mm. Both the studies performed measurements of water adsorption kinetics in Helium as a carrier gas since it is not adsorbed in silica gels. The presence of a second gas could hamper the utilisation of the mass transfer coefficient in systems were only water vapour is present. Brandani and Mangano [26] remarked how in their silica gel transport should only be a combination of Knudsen flow and surface diffusion. According to Brandani and Mangano [26] the mass transfer coefficient obtained can be used in systems with only water vapour present. In this study, a multi-parametric polynomial correlation was regressed from data of Brandani and Mangano [26], although results were always compared against those obtained with the eq. (11) from Goyal et al. [27], obtaining in all the experiments described below negligible discrepancies. Given the uncertainty in the diffusion, this study also considers instantaneous equilibrium, to constraint the results in a range of variability, between a minimum and a maximum.

Thermal response of the operating wet adsorber

The experimental test rig distribute hot or cold water at three temperature levels: *Cold* (set point range 10-27°C), *Amb* (set point range 20-30°C), and *Hot* (set point 60°C in this work). The identification of the adsorber dynamics was assessed on three different reduced temperatures $\Delta T_{Red} = (T_{cond,in} - T_{ev,in})/(T_{hot,in} - T_{cond,in})$, where $T_{cond,in}$ is the temperature of the condenser inlet, $T_{ev,in}$ is the temperature of the evaporator inlet and $T_{hot,in}$ the regeneration temperature at the adsorber inlet. The analysis of the performance as a function of ΔT_{Red} allows the generalisation of results from a limited range of combinations of the triplet ($T_{hot,in}$; $T_{cond,in}$; $T_{ev,in}$) to virtually all combinations without direct tests. This has been experimentally confirmed in diverse laboratories.[11,28,29] With this approach, the regeneration temperature can

be maintained constant in all experiments without hampering the applicability of the results to other regeneration temperatures.

The overall adsorber heating power was measured at three different reduced temperatures ΔT_{Red} = (0.56; 0.36; 0.15) at same inlet regeneration and condensation temperatures ($T_{hot,in}$; $T_{cond,in}$) = (56.5°C; 29.2°C) by varying the inlet evaporator temperatures at (13.8°C; 19.4°C; 25.1°C). Fig. 5 distinguishes the contribution of the sensible and non-sensible heat in the overall heat consumed in the adsorber at ΔT_{Red} = 0.56. When subject to a sudden increase of temperature (inlet temperature step-change), the heating power depends on ΔT_{Red}. The lowering of ΔT_{Red} (i.e. close condensation and evaporation temperatures, typical of adsorption desalination operational conditions) produces higher heating power peaks and amplitudes of both the sensible and non-sensible heat, although the heat of desorption increases more than the sensible heat. Fig. 5 shows the contributions of the sensible heat and non-sensible heat (mostly heat of desorption), by using the experimental data of pressure and temperatures in the eqns (8), (9) and (10).

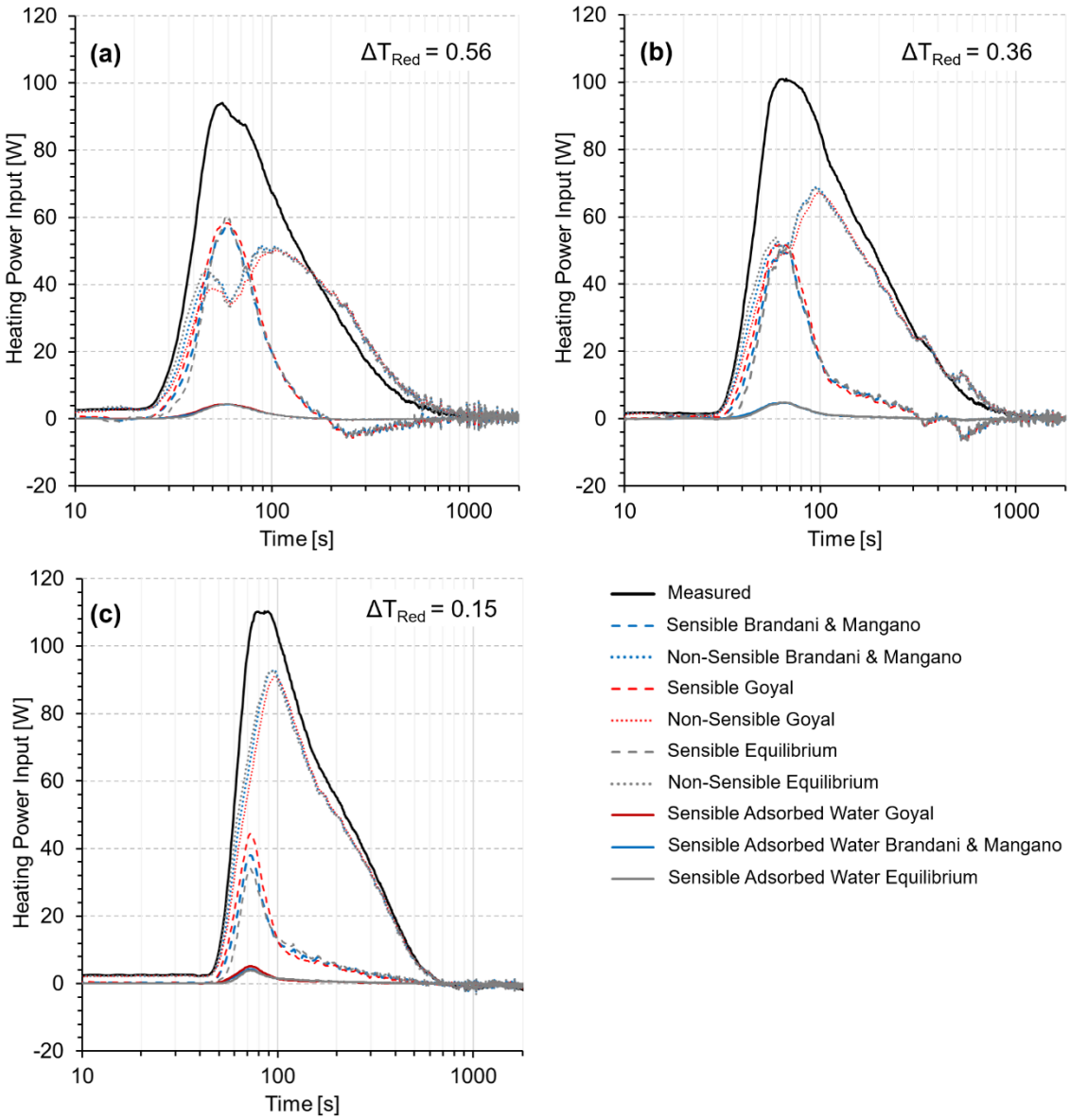

Figure 5: Heating Powers at ΔT_{Red} = 0.56 (a), ΔT_{Red} = 0.36 (b) and ΔT_{Red} = 0.15 (c) from temperature step-change experiments until steady-state (1800s) with contributions from the sensible heat (dashed) and heat not accountable as sensible (dotted) using the mass transfer coefficient from two different laboratories (red: Goyal et al. [27]; blue: Brandani and Mangano [26])

The patterns clearly highlight the existence of two overlapping periods with a trend across the reduced temperatures. At high ΔT_{Red} (cooling mode) it is more evident. In the first period, the heat exchanged is mostly sensible with a smaller contribution from the heat of desorption. In the second period, after achieving the peak of power, the total heating power decreases and the heat input is mostly used for desorbing water. The trend shows a counter-intuitive sensible cooling after about 180 seconds caused by a fall in pressure (Fig. SI3 Supplemental

Information) — corresponding to a temperature decrease of the saturated water vapour. Sensible cooling lasts until the end of the test and is caused by the convective heat transfer between cold water vapour and the metal heat exchanger.

The contribution of the heat of desorption increases progressively, until the two periods cannot be distinguished any longer at low ΔT_{Red} (desalination mode, Fig. 7 right). The contributions of sensible heat and heat of adsorption to the overall heat exchanged in Table 4 show energy is mostly spent on desorbing water, while a smaller percentage goes as sensible heat. The share the non-linear term $\left(\frac{\tau_{dry-ads}}{c_{p,eff,dry-ads}} - \frac{\tau_{HEX}}{c_{p,effHEX}}\right) c_{p,satliq,w} q(t) \frac{dT(t)}{dt}$ has on the overall heat consumed ranges from 1.3% to 1.5% of the total heat used in the adsorber, a contribution that could for this adsorber be neglected in the energy balance of eq. (8), reducing but not eliminating its non-linearity.

Table 4: Energy partitions in temperature step-change experiments using the mass transfer coefficient from Brandani and Mangano [26].

ΔT_{Red}	0.56	0.36	0.15
Overall Heating [kJ]	19.18 ± 0.89	22.13 ± 1.02	20.96 ± 0.97
Overall Cooling [kJ]	– 1.98 ± 0.09	– 1.21 ± 0.06	– 1.09 ± 0.05
Sensible Heat - Heating [kJ]	3.48 ± 0.16	3.66 ± 0.17	2.74 ± 0.13
Sensible Heat - Cooling [kJ]	– 1.62 ± 0.07	– 1.13 ± 0.05	– 0.40 ± 0.02
Sensible Heat Adsorbed Water - Heating [kJ]	0.25 ± 0.01	0.33 ± 0.02	0.30 ± 0.01
Sensible Heat Adsorbed Water - Cooling [kJ]	– 0.08 ± 0.004	– 0.08 ± 0.004	– 0.08 ± 0.004
Heat of Desorption [kJ]	15.70 ± 1.03	18.47 ± 1.21	18.22 ± 1.19
Heat of Adsorption [kJ]	– 0.37 ± 0.02	negligible	– 0.69 ± 0.05
Sensible Heat - Heating [%]	18.1	16.7	13.0
Heat of Desorption [%]	81.9	83.3	87.0

Note: Error analysis is in the Supplemental Information.

Unit Operation

Additional tests of continued operation showed that the evaporator outlet temperature crosses the inlet temperature (Fig. 6 left), an unwanted effect that reduces the module cooling power. The temperature difference in the evaporator reduces cycle after cycle, indicating a further reduction of the cooling.

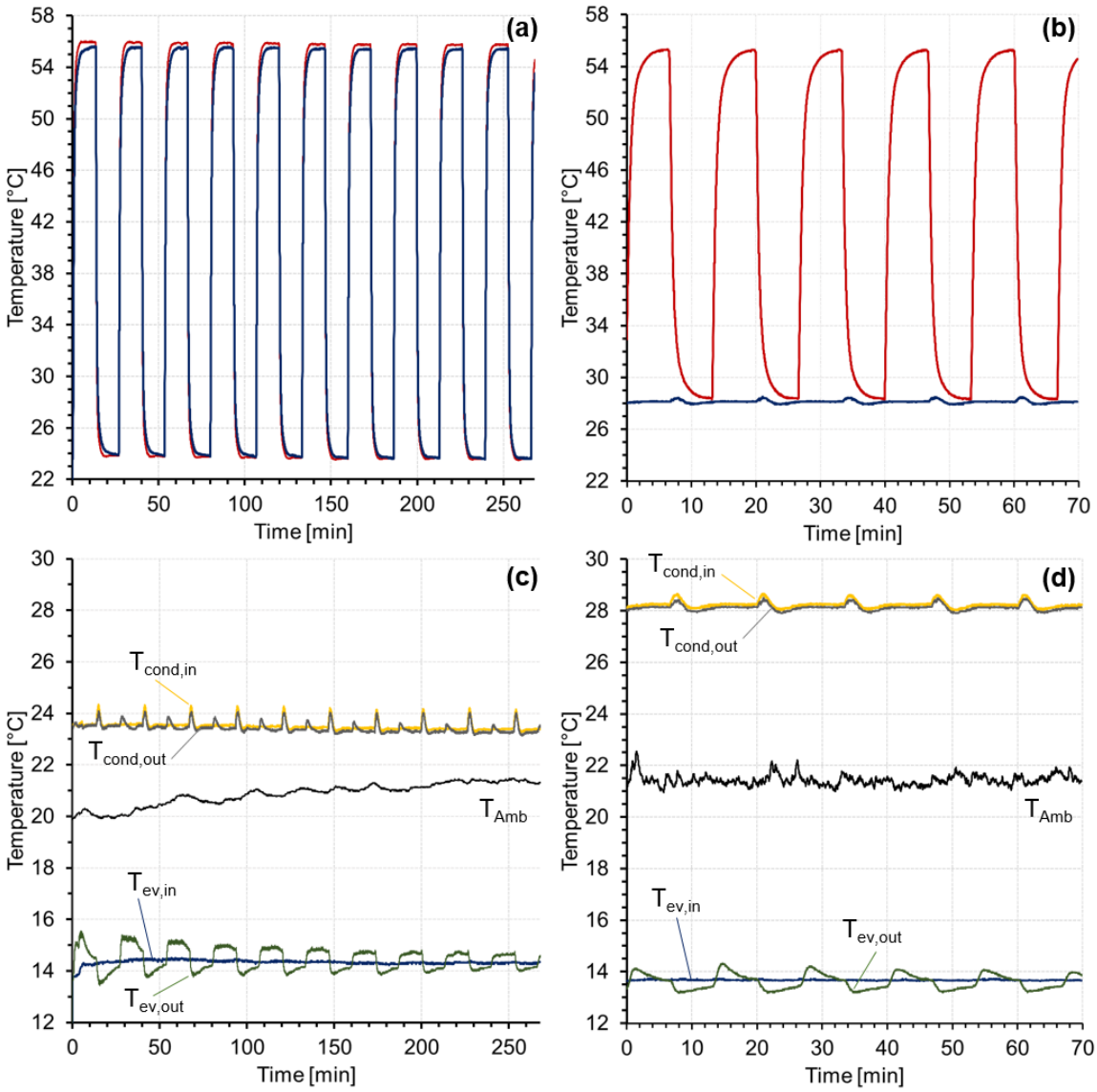

Figure 6: Trends of the inlet and outlet temperatures in the three heat exchangers along with the ambient temperature during multiple cycles testing at ΔT_{Red} = 0.52 in the initially designed unit, in (a) and (c), and at ΔT_{Red} = 0.51 in the same unit with reduced internal void volume, in (b) and (d). The pattern of the outlet evaporator temperature in (d) is constantly under the inlet evaporator temperature during adsorption.

The issue is caused by the magnitude of the void volume in the upper part of the module. In each cycle, part of the water vapour is re-adsorbed from the void volume instead of flowing through the condenser to the evaporator. The issue can be significantly mitigated by reducing the void volume. By reducing this volume (Fig. SI4 in Supplemental Information), the evaporator temperature trends (Fig. 6 right) show a larger cooling effect during adsorption. Fig. 7 compares the pressure trends one of the tests on the module soon after its construction (Fig. 7 left) and after two months (Fig. 7 right). The pressure trend is classifiable as very tight

[18], hence meeting the expectation of a unit of commercial quality after its construction. The pressure trends in Fig. 11 right, two months after construction, show a first range of cycles still classifiable as very tight, gradually moving towards higher pressure ranges classifiable as tight.[18] The decrease in vacuum tightness does not compromise the laboratory operation since the increase of pressure remains limited enough to allow testing. The decrease in tightness is because of a deterioration of the silicon sealing with time, indicating that other sealing materials (epoxy or acrylate) and techniques for the metal/plastic contacts would be more suitable to ensure long lasting tightness.

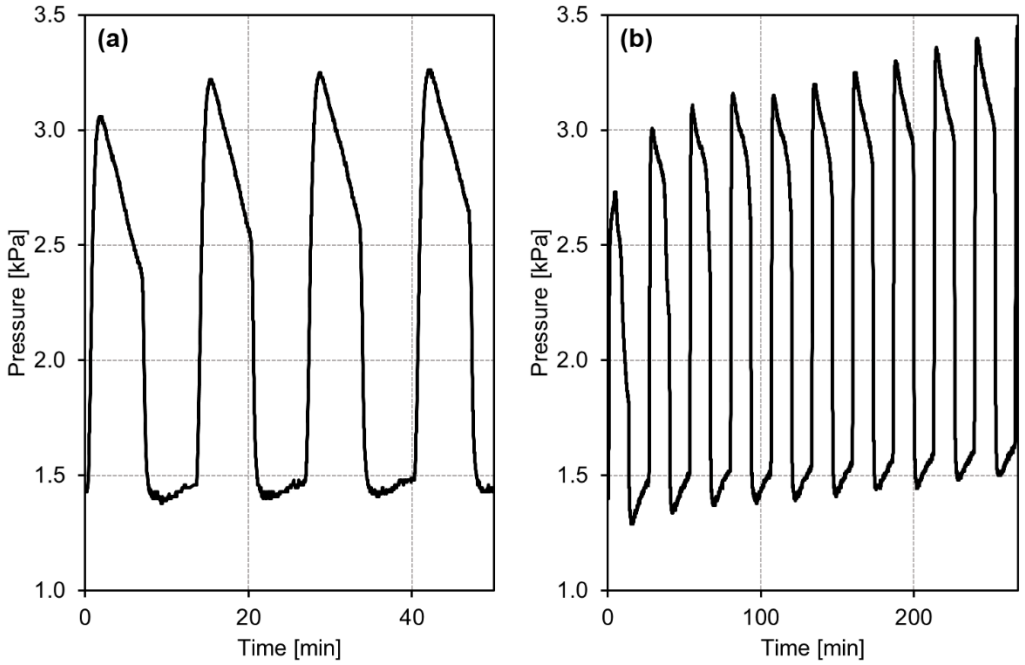

Figure 7: Pressure swings on just-built prototype (a) and on the same prototype after two months (b)

In this new configuration, the adsorption material follows the specific thermodynamic cycle in Fig. 8 that differs from the conventional cycle made of two isobars and two isosteres because of the constant volume across all temperature and pressure changes. Two transformations at constant uptake in heating and cooling and one isobar in cooling (during adsorption) compose the thermodynamic cycle, with the desorption transformation resembling an isotherm transformation and favouring higher performance. By working in part at constant temperature, the Coefficient of Performance of the unit is expected to be closer to a three temperatures Carnot cycle.[4]

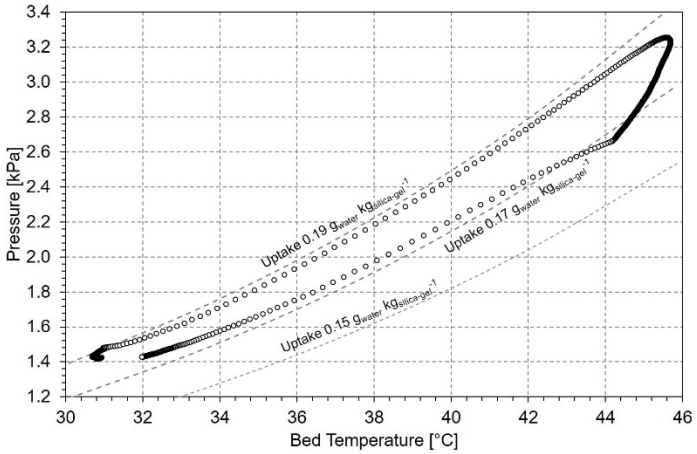

Figure 8: Silica gel thermodynamic cycle in the original configuration (no void volume reduction) at 400s half-cycle time. The temperature of the adsorption bed is assessed from eq. (8).

Coefficient of Performance (*COP*) and Specific Cooling Power (*SCP*) in [W $kg_{adsorbent}^{-1}$] are the indicators best capturing the performance of an adsorption chiller. By combining the definition of *SCP* and *COP* with the energy balance around the module, the *COP* is rewritten as (justification in the Supplemental Information):

$$COP = \frac{1}{1+\frac{|Q_{cond}|}{m_{adsorbent}\,\Delta t_{cycle}\,SCP}} \tag{12}$$

Where Q_{cond} in [J] is the energy exchanged at the condenser across the cycle, Δt_{cycle} in [s] the duration of one cycle. Eq. (12) clarifies how high *SCP* and *COP* are correlated and must be paired to show how their trade-off changes with a change of the operating conditions. In Fig. 9, the experimental {COP; SCP} pairs have been measured at different ΔT_{Red} representative of cooling at ΔT_{Red} = 0.51 from {$T_{hot,in}$; $T_{cond,in}$; $T_{ev,in}$} = {56.5°C; 28.3°C; 13.8°C}, desalination at ΔT_{Red} = 0.11 from {$T_{hot,in}$; $T_{cond,in}$; $T_{ev,in}$} = {56.5°C; 28.3°C; 25.1°C } and intermediate at ΔT_{Red} = 0.31 from {$T_{hot,in}$; $T_{cond,in}$; $T_{ev,in}$} = {56.5°C; 28.3°C; 19.4°C}, screening a large range of half-cycle times. The curves of the design with reduced void volume match the expected trends confirmed elsewhere by other laboratories.[30]

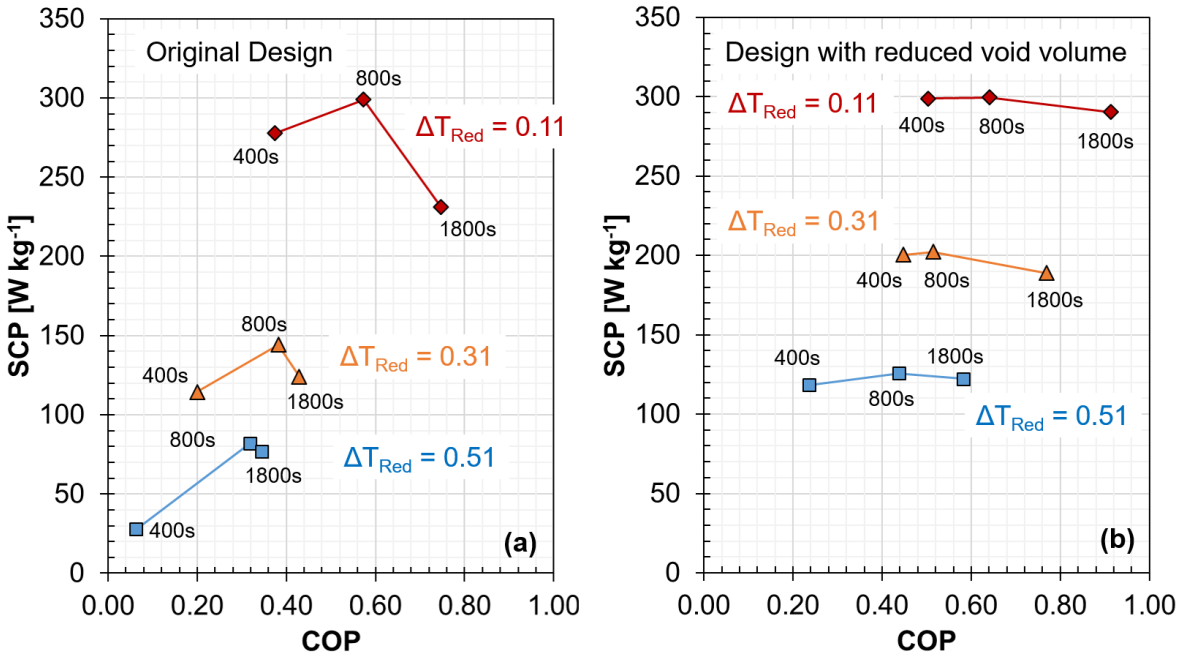

Figure 9: {*COP*; *SCP*} pair in different operating conditions of the original design (a) and the design with reduced void volume (b). $\Delta T_{Red} = (T_{cond,in} - T_{ev,in})/(T_{hot,in} - T_{cond,in})$. $\Delta T_{Red} = 0.11$ resembles conditions typical of adsorption desalination, $\Delta T_{Red} = 0.51$ resembles process conditions typical of adsorption cooling and $\Delta T_{Red} = 0.31$ resembles intermediate conditions between cooling and desalination.

The comparison of the reduced void volume module's performance with other experimental Silica gel chillers in Fig. 10 shows the device can work with regeneration temperatures lower than all the other proven adsorption chillers (higher ΔT_{Red}). When operated at the same ΔT_{Red} of the other chillers, the device provides better trade-offs between COP and SCP.

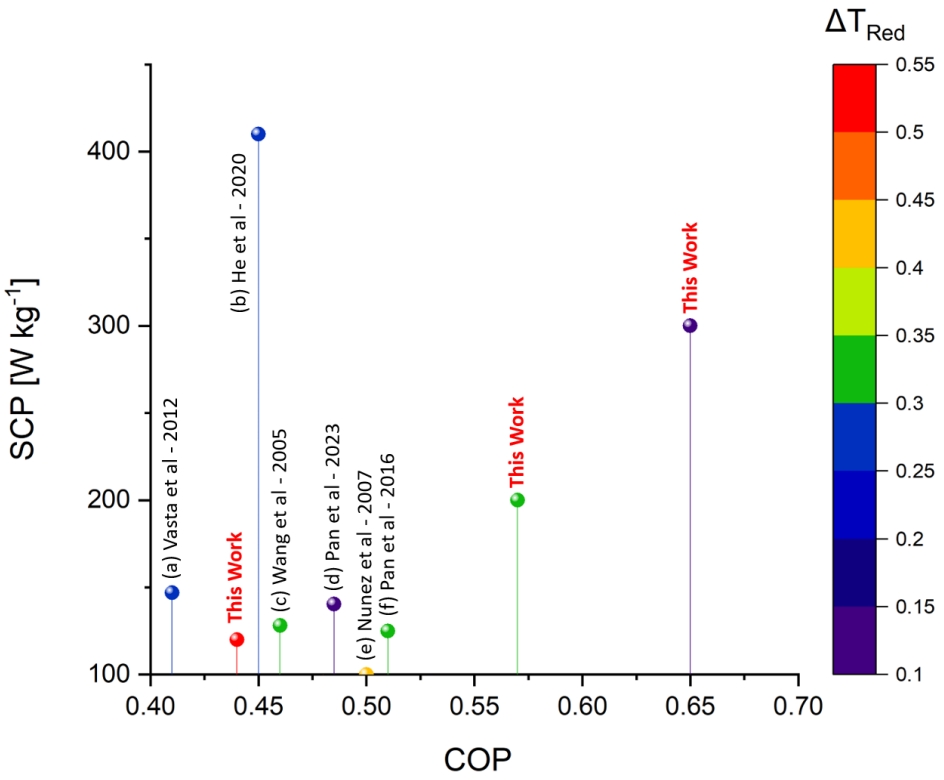

Figure 10: Comparison of the performance with other experimental Silica gel adsorption chillers. Only devices showing {COP; SCP} > {0.4; 100 W kg^{-1}} have been included. (a) Vasta et al - 2012;[31] (b) He et al - 2020;[32] (c) Wang et al - 2005;[33] (d) Pan et al - 2023;[34] (e) Nunez et al - 2007;[28] (f) Pan et al – 2016;[35] .

Conclusions

Stereolithographic 3D-printing of plastics was trialled at small scale in a silica gel adsorption chiller module and showed sufficient tightness for experimentation, with performance aligned with the current state-of-the art but standing out for its capability to usefully transform ultralow grade heat into cold. The valveless miniature proof-of-principle design gathers all heat exchangers in one 3D-printed plastic enclosure. In this new configuration the adsorption material follows an unconventional thermodynamic cycle. The thermal response method, which assumes the adsorption bed is a linear dynamic system, was extended to take into account the non-linearity of the adsorber dynamics with higher fidelity and mitigate energy partition misallocations. Manufacturing adsorption cooling modules in 3D-printing opens to quicker and more affordable, easily replicable research and development. The new possibilities enabled by 3D printing in adsorption cooling need to be pursued further towards simple modules containing more 3D-printed parts than the only vessel, to exploit in full the

opportunity of designing heat exchangers free from the constraints of the usual manufacturing methods and able to operate with optimal mass transfer.

Acknowledgements

We thank the Sultanate of Oman government, Ministry of Higher Education, Research and Innovation and The University of Edinburgh for supporting the studentship of Shihab AL-Hasni and the Royal Academy of Engineering for the industrial fellowship of Giulio Santori in Industrial-scale manufacturing of heat-powered chillers for energy efficient data centres (IF2223B-126).

Nomenclature

$(m\ c_p)_{dry-ads}$	Heat capacity rate of the dry adsorber [J K^{-1}]
$(m\ c_p)_{HEX}$	Heat capacity rate of the heat exchanger without adsorption material (naked) [J K^{-1}]
$(\dot{m}\ c_p)_{htf}$	Heat capacity rate of the heat transfer fluid [W K^{-1}]
COP	Coefficient of Performance [-]
$c_{p,effHEX}$	Effective specific heat capacity of heat exchanger [J kg^{-1} K^{-1}]
$c_{p,sg,dry}$	Specific heat capacity of dry silica gel [J kg^{-1} K^{-1}]
$c_{p,eff,dry-ads}$	Effective specific heat capacity of dry adsorber [J kg^{-1} K^{-1}]
$c_{p,satliq,w}$	Specific heat capacity of saturated liquid water [J kg^{-1} K^{-1}].
$D_{s,0}$	Pre-exponential constant of the mass transfer coefficient model [m^2 s^{-1}]
E	Dubinin–Astakhov isotherm parameter [kJ mol_{water}^{-1}]
E_a	Activation energy of the mass transfer coefficient model [kJ mol^{-1}]
h_{ads}	Differential heat of water adsorption on Siogel silica gel [J kg_{water}^{-1}]
in	Inlet
K	Mass transfer coefficient [s^{-1}]
$\dot{m}$	Water mass flow rate [kg s^{-1}]
$m_{adsorbent}$	Dry mass of the adsorbent material loaded in the adsorption bed [kg]
$m_{dry-ads}$	Total dry adsorber weight [g]
n	Dubinin-Astakov exponent constant
N_1; N_2; N_3	Integral over time of temperature difference [K s] used to obtain time constants
out	Outlet
P_{exp}	Experimental pressure acquired during the tests [kPa]
P_{sat}	Saturation pressure of water at the adsorber temperature [kPa]
$q(t)$	The actual time-dependent uptake [mol_{water} $mol_{sg,\ dry}^{-1}$]
Q_{ev}	The cooling energy produced at the evaporator [J]
$Q_{heating}$	The heating energy consumed at the adsorber [J]
$q_{eq}(t)$	The time-dependent equilibrium uptake [mol_{water} $kg_{sg,dry}^{-1}$]
q_s	Siogel silica gel maximum water saturation uptake [mol_{water} $kg_{sg,dry}^{-1}$]
R	Universal gas constant [kJ mol^{-1} K^{-1}]
SCC	Specific cooling capacity [J $kg_{adsorbent}^{-1}$]
SCP	Specific cooling power [W $kg_{adsorbent}^{-1}$]
$T_{dry-ads}(t)$	Time-dependent overall temperature of the adsorber without adsorption (dry condition) [K]
$T_{HEX}(t)$	Time-dependent overall temperature of the heat exchanger [K]
T_{in}	Experimental inlet temperature [K]
$T_{out}(t)$	Experimental outlet temperature as a function of time [K]
T_{cond}	Condenser temperature [°C]
T_{ev}	Evaporator temperature [°C]
T_{hot}	Maximum experimental temperature of the adsorber bed at the end of the heating [°C]
τ_{HEX}	Time constant of the heat exchanger without adsorption material (naked) [s]
$\tau_{dry-ads}$	Time constant of the dry adsorption bed [s]
ΔT_{red}	Reduced temperature [-]
Δt_{cycle}	Cycle time [seconds]
ΔT_{in1}; ΔT_{in2} ΔT_{in3}	Temperature step changes [K] used to obtain time constants

References

1. Veselovskaya, J. V., Tokarev, M.M., and Aristov, Y.I. (2010). Novel ammonia sorbents “porous matrix modified by active salt” for adsorptive heat transformation. 1. Barium chloride in various matrices. Applied Thermal Engineering *30*, 584–589. 10.1016/j.applthermaleng.2009.11.001.

2. Luberti, M., Gowans, R., Finn, P., and Santori, G. (2022). An estimate of the ultralow waste heat available in the European Union. Energy *238*, 121967. 10.1016/j.energy.2021.121967.

3. Aristov, Y.I. (2021). Adsorptive conversion of ultralow-temperature heat: Thermodynamic issues. Energy *236*. 10.1016/j.energy.2021.121892.

4. Meunier, F., Neveu, P., and Castaing-Lasvignottes, J. (1998). Equivalent Carnot cycles for sorption refrigeration. International Journal of Refrigeration *21*, 472–489. 10.1016/S0140-7007(97)00084-4.

5. Wang, R., Wang, L., and Wu, J. (2014). Adsorption Refrigeration Technology: Theory and Application. Adsorption Refrigeration Technology: Theory and Application *9781118197431*, 1–494. 10.1002/9781118197448.

6. Boman, D.B., Raymond, A.W., and Garimella, S. (2021). Adsorption Heat Pumps (Springer International Publishing) 10.1007/978-3-030-72180-0.

7. eCoo S - FAHRENHEIT https://fahrenheit.cool/produkt/ecoo-s/.

8. Adsorption Chiller - Innovative Green Technology | Bry- Air https://www.bryair.com/products-solutions/adsorption-chillers/adsorption-chiller/.

9. AL-Hasni, S., and Santori, G. (2023). The cost of manufacturing adsorption chillers. Thermal Science and Engineering Progress *39*, 101685. 10.1016/j.tsep.2023.101685.

10. Maher, H., Rupam, T.H., Rocky, K.A., Bassiouny, R., and Saha, B.B. (2021). Silica gel-MIL 100(Fe) composite adsorbents for ultra-low heat-driven atmospheric water harvester. Energy *238*. 10.1016/j.energy.2021.121741.

11. Olkis, C., Brandani, S., and Santori, G. (2019). Cycle and performance analysis of a small-scale adsorption heat transformer for desalination and cooling applications. Chemical Engineering Journal *378*, 122104. 10.1016/j.cej.2019.122104.

12. Martínez, P.J., Martínez, P., Soto, V.M., Bujedo, L.A., and Rodriguez, J. (2020). Design of a 35 kW Solar Cooling Demonstration Facility for a Hotel in Spain. Applied Sciences 2020, Vol. 10, Page 496 *10*, 496. 10.3390/APP10020496.

13. Mugnier, D., Neyer, D., and White, S.D. (2017). The Solar Cooling Design Guide - Case Studies of Successful Solar Air Conditioning Design. The Solar Cooling Design Guide - Case Studies of Successful Solar Air Conditioning Design. 10.1002/9783433606841.

14. U.S. Department of Energy - Advanced Manufacturing Office (2017). Combined Heat and Power Technology Fact Sheet Series - Absorption Vhillers CHP Systems. DOE/EE-1608.

15. Vasta, S., Palomba, V., Frazzica, A., Di Bella, G., and Freni, A. (2016). Techno-Economic Analysis of Solar Cooling Systems for Residential Buildings in Italy. Journal of Solar Energy Engineering *138*, 031005. 10.1115/1.4032772.

16. Soo, A., Ali, S.M., and Shon, H.K. (2021). 3D printing for membrane desalination: Challenges and future prospects. Desalination *520*, 115366. 10.1016/J.DESAL.2021.115366.

17. Sapienza, A., Brancato, V., Aristov, Y., and Vasta, S. (2021). Plastic heat exchangers for adsorption cooling: Thermodynamic and dynamic performance. Applied Thermal Engineering *188*, 116622. 10.1016/j.applthermaleng.2021.116622.

18. AL-Hasni, S., and Santori, G. (2020). 3D printing of vacuum and pressure tight polymer vessels for thermally driven chillers and heat pumps. Vacuum *171*, 109017. 10.1016/j.vacuum.2019.109017.

19. Olkis, C., Brandani, S., and Santori, G. (2019). Design and experimental study of a small scale adsorption desalinator. Applied Energy *253*, 113584. 10.1016/j.apenergy.2019.113584.

20. Product-Cost-Calculation for EXCEL https://www.calc4xl.com/en/home/.

21. Gluesenkamp, K.R., Frazzica, A., Velte, A., Metcalf, S., Yang, Z., Rouhani, M., Blackman, C., Qu, M., Laurenz, E., Rivero-Pacho, A., et al. (2020). Experimentally Measured Thermal Masses of Adsorption Heat Exchangers. Energies 2020, Vol. 13, Page 1150 *13*, 1150. 10.3390/EN13051150.

22. Tokarev, M.M., and Aristov, Y.I. (2017). A new version of the Large Temperature Jump method: The thermal response (T–LTJ). Energy *140*, 481–487. 10.1016/J.ENERGY.2017.08.093.

23. Tokarev, M.M., Zlobin, A.A., and Aristov, Y.I. (2019). A new version of the large pressure jump (T-LPJ) method for dynamic study of pressure-initiated adsorptive cycles for heat storage and transformation. Energy *179*, 542–548. 10.1016/J.ENERGY.2019.04.164.

24. Olkis, C., Santori, G., and Brandani, S. (2018). An Adsorption Reverse Electrodialysis system for the generation of electricity from low-grade heat. Applied Energy *231*, 222–234. 10.1016/J.APENERGY.2018.09.112.

25. Sapienza, A., Velte, A., Girnik, I., Frazzica, A., Füldner, G., Schnabel, L., and Aristov, Y. (2017). "Water - Silica Siogel" working pair for adsorption chillers: Adsorption equilibrium and dynamics. Renewable Energy *110*, 40–46. 10.1016/J.RENENE.2016.09.065.

26. Brandani, S., and Mangano, E. (2022). Direct measurement of the mass transport coefficient of water in silica-gel using the zero length column technique. Energy *239*. 10.1016/j.energy.2021.121945.

27. Goyal, P., Purdue, M.J., and Farooq, S. (2020). Adsorption and diffusion of moisture and wet flue gas on silica gel. Chemical Engineering Science *227*, 115890. 10.1016/J.CES.2020.115890.

28. Núñez, T., Mittelbach, W., and Henning, H.-M. (2007). Development of an adsorption chiller and heat pump for domestic heating and air-conditioning applications. Applied Thermal Engineering *27*, 2205–2212. 10.1016/J.APPLTHERMALENG.2005.07.024.

29. Núñez, T., Mittelbach, W., and Henning, H.-M. (2006). Development of a Small-Capacity Adsorption System for Heating and Cooling Applications. HVAC&R Research *12*, 749. 10.1080/10789669.2006.10391205.

30. Bau, U., Hoseinpoori, P., Graf, S., Schreiber, H., Lanzerath, F., Kirches, C., and Bardow, A. (2017). Dynamic optimisation of adsorber-bed designs ensuring optimal control. Applied Thermal Engineering *125*, 1565–1576. 10.1016/J.APPLTHERMALENG.2017.07.073.

31. Vasta, S., Freni, A., Sapienza, A., Costa, F., and Restuccia, G. (2012). Development and lab-test of a mobile adsorption air-conditioner. International Journal of Refrigeration *35*, 701–708. 10.1016/j.ijrefrig.2011.03.013.

32. He, F., Nagano, K., and Togawa, J. (2020). Experimental study and development of a low-cost 1 kW adsorption chiller using composite adsorbent based on natural mesoporous material. Energy *209*, 118365. 10.1016/j.energy.2020.118365.

33. Wang, X., Chua, H.T., and Ng, K.C. (2005). Experimental investigation of silica gel–water adsorption chillers with and without a passive heat recovery scheme. International Journal of Refrigeration *28*, 756–765. 10.1016/j.ijrefrig.2004.11.011.

34. Pan, Q.W., Liu, L., Wang, B., Xu, J., and Ge, T.S. (2023). Design and experimental study on a small-scale silica gel/water adsorption chiller with heat and mass recovery scheme for solar energy use. Solar Energy *252*, 91–100. 10.1016/j.solener.2023.01.052.

35. Pan, Q.W., Wang, R.Z., Wang, L.W., and Liu, D. (2016). Design and experimental study of a silica gel-water adsorption chiller with modular adsorbers. International Journal of Refrigeration *67*, 336–344. 10.1016/j.ijrefrig.2016.03.001.